Power Engineering and Engineering Thermophysics
https://www.acadlore.com/journals/PEET

Natural Convection Flow in a Thermally Stratified Fluid Through an Asymmetrically Heated and Cooled Vertical Channel with Anisotropic Porous Material

Basant K. Jha, Muhammad K. Musa*, Abiodun O. Ajibade

Department of Mathematics, Ahmadu Bello University, 810241 Zaria, Nigeria

* Correspondence: Muhammad K. Musa (mmkabirxy@yahoo.com)

Received: 04-23-2024 **Revised:** 06-14-2024 **Accepted:** 06-22-2024

Citation: B. K. Jha, M. K. Musa, and A. O. Ajibade, "Natural convection flow in a thermally stratified fluid through an asymmetrically heated and cooled vertical channel with anisotropic porous material," *Power Eng. Eng. Thermophys.*, vol. 3, no. 2, pp. 116–133, 2024. https://doi.org/10.56578/peet030204.

Abstract: The study aimed to compare the effects of thermal stratification (S), anisotropic parameters (k^* and θ), and buoyancy force distribution parameter (m^*) on natural convection in fluids characterized by high and low Prandtl numbers. The second-order coupled partial differential equations governing the problem were initially converted into ordinary differential equations through the Laplace transform technique. The D'Alembert method was then applied to systematically decouple these equations without altering their original order. Subsequently, the closed-form solutions in the Laplace domain were transformed into their respective time domains using a numerical scheme based on the Riemann sum algorithm. The research established that reverse flow is feasible under certain conditions, occurring more rapidly in fluids with lower Prandtl numbers. Additionally, it was observed that an increase in k^* and S reduces skin friction on the bounding plates, whereas an increase in θ enhances skin friction on both channel walls.

Keywords: D'Alembert method; Riemann sum approximation; Laplace transform techniques; Anisotropic porous material; Thermal stratification; Buoyancy force distribution; Prandtl number

1 Introduction

The study of transport phenomena of thermally stratified fluids flowing through porous passages, characterized by non-uniform permeabilities driven by asymmetric heating and cooling of the surfaces of transport media, holds significant applications in industries and various natural processes. It is observed that these phenomena frequently coexist in natural settings and are integral to technological advancements; however, a tendency is noted among researchers to investigate the impacts of these physical phenomena in isolation [1].

Natural convection and heat transfer through porous media find crucial applications in geothermal exploitation, management of radioactive waste, agricultural engineering, and environmental sciences. After noting the utilization of transport theory in porous media, Khaled and Vafai [2] used mathematical models like Darcy and Brinkman equations to investigate fluid flow and heat transfer in biological tissues, providing insights into understanding fluid flow in biological systems. Govindaraju et al. [3] took mammalian blood as a non-Newtonian fluid and the human coronary artery as the transport medium with permeable walls by utilizing the Darcy-Forchheimer model, highlighting the influence of stenotic arterial walls on blood flow properties. Das et al. [4] studied blood flow dynamics through porous structures by incorporating realistic blood rheology and pulsatile motion, revealing the impact of coil embolization on wall shear and pressure.

Recent works, such as the investigation by Khanafer and Vafai [5], document the diverse applications of porous media in biological systems. Researchers have demonstrated that leveraging the conductivity and non-uniform permeabilities of porous structures, such as fibers or grains, can lead to optimal applications. Anisotropy arises from the non-uniform distribution, fractural structure, and preferential orientation of porous material beads [6]. Compared to isotropic porous matrices with scalar permeability, anisotropic porous structures exhibit tensor permeability, characterized by the ratio of permeability $\left(k^*=\frac{k_1}{k_2}\right)$ and the orientation angle (θ) between transverse distance (y) and horizontal permeability (k_2). The structural tensor form of anisotropic porous matrix permeability offers intriguing applications, such as the fabrication of porous titanium with square pores for trabecular bone implants [7].

Garcia-Avila et al. [8] conducted a comparative mathematical simulation, revealing higher fatigue resistance properties of non-cubic porous materials compared to normal triply periodic minimal surface (TPMS).

In most previous investigations, cases where the ambient medium outside the flow region is isothermal and of uniform density have been primarily considered in flow configurations. However, this present study takes into account flow formation with non-uniform fluid density in the ambient medium, varying with height, a common occurrence resulting from heat or mass transfer processes. Stratification, as characterized by the combined effects of ambient fluid temperature or vertical advection and reversible work done on fluid particles by compression, has garnered significant interest among researchers for studying variable environmental conditions [9–14].

The coupled mathematical model addressing the combined effects of anisotropy and stratification, as previously investigated by Jha et al. [15], focuses on the convective interplay between fluid particles and constituents of anisotropic porous structures. However, the orientation of the surface temperature of transport media with respect to the fluid temperature flowing through anisotropic porous material remains grossly underexplored. Therefore, this present study not only considers anisotropy and stratification but also examines the effect of asymmetric heating and cooling of transport channel walls. Including asymmetric heating and cooling constraints in the mathematical model captures real-world convective processes, such as variation in environmental conditions and heating and warming of the human body [16]. Additionally, Peng et al. [17] investigated the behavior of the surface temperature of transport media with respect to fluid temperature, highlighting the intriguing area of studying fabric materials that provide maximum comfort and better management of heat transport pathways from the human body to the ambient media.

2 Mathematical Model

Considering a one-dimensional, transient flow of a stratified fluid in the region $0 < y' < \mathrm{h}$ driven by the asymmetric heating and cooling of the channel walls, the channel is saturated with fibers or grains with non-uniform permeabilities. The physical configuration for this research is shown in Figure 1. In this set up, the x' axis was chosen along the channel walls and the y' axis normal to them. At $t' \leq 0$, the channel packed with anisotropic porous material and saturated with stratified fluids is all at the same local thermodynamic equilibrium. At time $t' > 0$, it is assumed that the temperature of channel walls $y' = 0$ and $y' = h$ are instantaneously raised or lowered to $T' = T_h$ or $T' = T_c$, respectively.

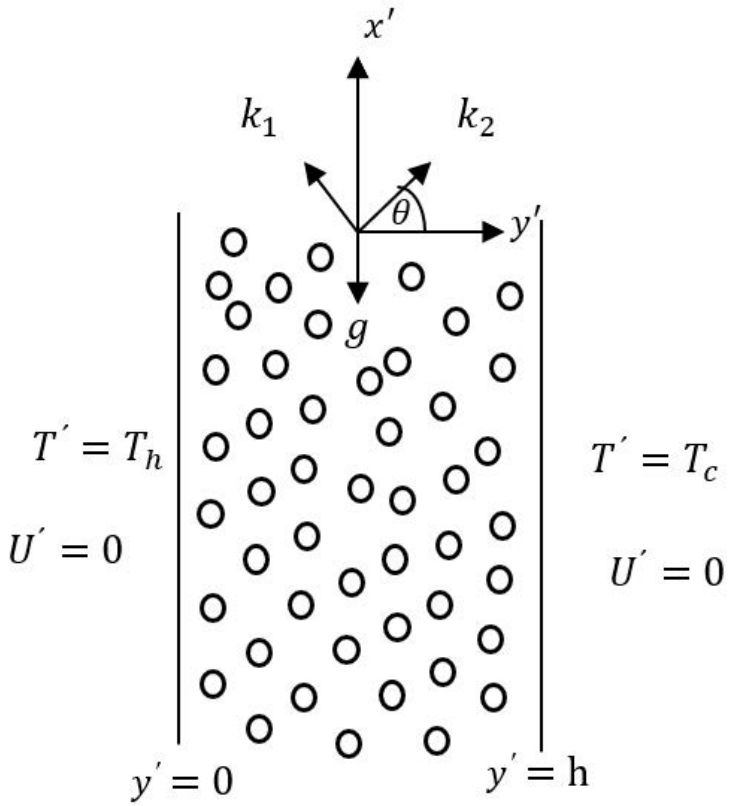

Figure 1. Schematic diagram depicting the configuration and the coordinates system of the problem

The fully developed one-dimensional time-dependent governing mathematical model representing the present problem is predicated based on the following assumptions:

(i) The fluid flows through a porous structure that is anisotropic in nature so that the variant directional inclinations of the permeabilities of the porous matrix are taken into account [18].

(ii) The vertical transport medium is filled with stratified fluids of low and high Prandtl numbers. Such fluids arise from inhomogeneous fluid parcels of variable densities which, under the influence of gravitational pull, arrange themselves such that fluid parcels with higher densities are found beneath those with lower densities [9].

(iii) The onset of natural convection is induced by the asymmetric heating and cooling of the walls of the vertical channel. Such heating is characterized by the buoyancy force distribution quantity. Singh and Paul [16] discussed the categorizations of the cases of the buoyancy force distribution term. Thus, the momentum and energy equations resulting from the above assumptions are given in dimensional forms as follows:

$$\frac{\partial U'}{\partial t'} = v_{eff}\frac{\partial^2 U'}{\partial y'^2} - \frac{U'v}{\overline{\overline{K}}} + g\beta\left(T' - T_m\right) \tag{1}$$

$$\frac{\partial T'}{\partial t'} = \alpha\frac{\partial^2 T'}{\partial y'^2} - S'U' \tag{2}$$

where, $\alpha = \frac{k}{\rho c_p}$. And $\overline{\overline{K}}$ is the symmetrical second-order permeability tensor and is defined as follows:

$$\overline{\overline{K}} = \begin{bmatrix} k_1\sin^2(\theta) + k_2\cos^2(\theta) & (k_1 - k_2)\sin(\theta)\cos(\theta) \\ (k_1 - k_2)\sin(\theta)\cos(\theta) & k_2\sin^2(\theta) + k_1\cos^2(\theta) \end{bmatrix} \tag{3}$$

where, according to Liakopoulos [19], Eq. (3) physically characterizes the direction along which the fluid in an anisotropic porous system under a known imposed transport constraint flow.

In this study, the initial and boundary conditions consistent with the above model are as follows:

$$\begin{aligned} &t' \le 0, \quad T' = T_m, \quad U' = 0, \quad \text{for } 0 \le y' \le h \\ &t' > 0, \begin{cases} T' = T_h, U' = 0, & \text{at} \quad y' = 0 \\ T' = T_c, U' = 0 & \text{at} \quad y' = h \end{cases} \end{aligned} \tag{4}$$

In order to facilitate the mathematical analysis, the governing second-order coupled partial differential equations are non-dimensionalized using suitable transformational variables defined as follows:

$$U = \frac{U'\mathrm{h}}{v}, \quad T = \frac{T' - T_m}{T_h - T_m}, y = \frac{y'}{h}, \gamma = \frac{v_{eff}}{v}, t = \frac{t'v}{\mathrm{h}^2}, \mathrm{Pr} = \frac{v}{\alpha} \text{ and } Gr = \frac{g\beta\left(T_h - T_m\right)\mathrm{h}^3}{v^2}$$

The non-dimensionalization procedure shows that the characteristic stratification parameter S can be taken as $S = \frac{S'h}{T_h - T_m}$, and the measure of permeability of the anisotropic porous passages is defined by $Da = \frac{k_1}{h^2}$.

Using the non-dimensional variables defined above, the transformed velocity and temperature equations in dimensionless form are thus expressed as follows:

$$\frac{\partial U}{\partial t} = \gamma\frac{\partial^2 U}{\partial y^2} - a\frac{U}{Da} + GrT \tag{5}$$

$$\frac{\partial T}{\partial t} = \frac{1}{Pr}\frac{\partial^2 T}{\partial y^2} - SU \tag{6}$$

where, a in Eq. (5) represents the anisotropic factor derived from Eq. (3) and is defined as follows:

$$a = \sin^2(\theta) + k^*\cos^2(\theta) \tag{7}$$

where, $k^* = \frac{k_1}{k_2}$ and θ are the anisotropic parameters.

The dimensionless initial and boundary conditions now take the following form:

$$t \leq 0, T = 0, U = 0, \text{for} \quad 0 \leq y \leq 1$$
$$t > 0 \begin{cases} T = 1, U = 0 & \text{at } y = 0 \\ T = m^*, U = 0 & \text{at } y = 1 \end{cases} \tag{8}$$

where, $m^* = \frac{T_c{}' - T_m}{T_h - T_m}$ represents the buoyancy force distribution parameter. It is interesting to note that $m^* = 0$ represents the classical case when the temperatures of the fluid (T_m) and that of the cool plate (T_c) are thermally equal but less than the temperature of the heated plate (T_h). While $m^* = 1$ symbolizes the case when $T_m < T_h = T_c$. In addition, $m^* < 0$ describes the case where the fluid temperature is in between the different plates' temperatures. Finally, $0 < m^* < 1$ characterizes the case where either the temperature of the heated plate T_h is fixed between the temperatures of the cooled plate (T_c) and the fluid's temperature (T_m) or the case where the temperature of the cooled plate (T_c) fits in between the temperatures of the heated plate (T_h) and the fluid's temperature (T_m).

2.1 Solution

Taking the Laplace transform with respect to time (t) to the partial differential Eqs. (5) and (6), subject to the initial condition in Eq. (8), the following ordinary differential equations are obtained:

$$\frac{d^2\bar{U}}{dy^2} - \frac{\bar{U}}{\gamma}\left(p + \frac{a}{Da}\right) = -Gr\frac{\bar{T}}{\gamma} \tag{9}$$

$$\frac{d^2\bar{T}}{dy^2} - SPr\bar{U} - p\bar{T}Pr = 0 \tag{10}$$

where, $p > 0$ is the Laplace parameter.

Since solving Eqs. (9) and (10) by the direct elimination of either the velocity or temperature can result in solving a fourth-order equation, the D'Alembert method [20, 21], which systematically uncouples a set of coupled equations while still retaining their initial orders, was employed. Accordingly, by adding the result of the integral multiple of Eq. (9) with F^* to Eq. (10) and simplifying the final equation, the following equation can be yielded:

$$\frac{d^2}{dy^2}\left(F^*\bar{U} + \bar{T}\right) - \Omega^{*2}\left(F^*\bar{U} + \bar{T}\right) = 0 \tag{11}$$

where, F^* and Ω^* are the D'Alembert quadratic functions defined as follows:

$$F^{*2} + \frac{F^*[(pDa + a) - pDa\gamma Pr]}{GrDa} + \frac{\gamma SPr}{Gr} = 0 \tag{12}$$

$$\Omega^{*2} - \frac{\gamma pPr - F^*Gr}{\gamma} = 0 \tag{13}$$

Thus, solving Eq. (11) gives the general solution of the model in the Laplace domain as follows:

$$F^*\bar{U} + \bar{T} = A_1\cosh\left(\Omega^* y\right) + A_2\sinh\left(\Omega^* y\right) \tag{14}$$

By applying the boundary conditions of Eq. (8) to Eq. (14), the constants A_1 and A_2 in Eq. (14) are calculated as follows:

$$A_1 = \frac{1}{p} \tag{15}$$

$$A_2 = -\frac{m^{**} - \cosh(\Omega)}{p\sinh(\Omega)} \tag{16}$$

Thus, the particular solution of Eq. (14) becomes as follows:

$$F^*\bar{U} + \bar{T} = \frac{[\sinh(\Omega^*(1-y)) + m^*\sinh(\Omega^* y)]}{p\sinh(\Omega^*)} \tag{17}$$

By using F_1^*, F_2^*, Ω_1^*, and Ω_2^*, the roots of the solutions of the quadratic expressions in Eqs. (12) and (13) derived and expressed as follows, respectively:

$$F_1^* = -\frac{1}{2}\left(\frac{p}{Gr} + \frac{a}{GrDa} - \frac{\gamma pPr}{Gr}\right) + \frac{1}{2}\left(\sqrt{\left(\frac{p}{Gr} + \frac{a}{GrDa} - \frac{\gamma pPr}{Gr}\right)^2 - \frac{4\gamma SPr}{Gr}}\right) \tag{18}$$

$$F_2^* = -\frac{1}{2}\left(\frac{p}{Gr} + \frac{a}{GrDa} - \frac{\gamma pPr}{Gr}\right) - \frac{1}{2}\left(\sqrt{\left(\frac{p}{Gr} + \frac{a}{GrDa} - \frac{\gamma pPr}{Gr}\right)^2 - \frac{4\gamma SPr}{Gr}}\right) \tag{19}$$

$$\Omega_1^* = \sqrt{\frac{\gamma pPr - F_1 Gr}{\gamma}} \tag{20}$$

$$\Omega_2^* = \sqrt{\frac{\gamma pPr - F_2 Gr}{\gamma}} \tag{21}$$

The expressions of the velocity and temperature fields are separately obtained and are given as follows:

$$\bar{U} = \frac{1}{p(F_1^* - F_2^*)}\left[\frac{(\sinh(\Omega_1^*(1-y)) + m^*\sinh(\Omega_1^* y))}{\sinh(\Omega_1^*)} - \frac{(\sinh(\Omega_2^*(1-y)) + m^*\sinh(\Omega_2^* y))}{\sinh(\Omega_2^*)}\right] \tag{22}$$

$$\bar{T} = \frac{1}{p(F_1^* - F_2^*)}\left[\frac{(F_1^*(\sinh(\Omega_2^*(1-y)) + m^*\sinh(\Omega_2^* y)))}{\sinh(\Omega_2^*)} - \frac{(F_2^*(\sinh(\Omega_1^*(1-y)) + m^*\sinh(\Omega_1^* y)))}{\sinh(\Omega_1^*)}\right] \tag{23}$$

2.2 Skin Friction and Mass Flow Rate

To estimate the quantitative effects of the various parameters involved in the results of the present analysis with respect to the velocity gradients at the channel walls and the amount of fluid passing through the anisotropic porous passages per unit area, the skin friction $\left(\bar{\tau} = \frac{d\bar{U}}{dy}\Big|_{y=0,1}\right)$ and volumetric mass flow $\left(\bar{Q}^* = \int_0^1 \bar{U}dy\right)$ are calculated and presented as follows, respectively:

$$\bar{\tau}_0 = \frac{1}{p(F_1^* - F_2^*)}\left[\frac{\Omega_1^*(m^* - \cosh(\Omega_1^*))}{\sinh(\Omega_1^*)} - \frac{\Omega_2^*(m^* - \cosh(\Omega_2^*))}{\sinh(\Omega_2^*)}\right] \tag{24}$$

$$\bar{\tau}_1 = \frac{1}{p(F_1^* - F_2^*)}\left[\frac{\Omega_1^*(m^*\cosh(\Omega_1^*) - 1)}{\sinh(\Omega_1^*)} - \frac{\Omega_2^*(m^*\cosh(\Omega_2^*) - 1)}{\sinh(\Omega_2^*)}\right] \tag{25}$$

$$\bar{Q}^* = \frac{1}{p(F_1^* - F_2^*)}\left[\frac{m^*(\cosh(\Omega_1^*) - 1) + \cosh(\Omega_1^*) - 1}{\Omega_1^*\sinh(\Omega_1^*)} + \frac{m^*(1 - \cosh(\Omega_2^*)) + 1 - \cosh(\Omega_2^*)}{\Omega_2^*\sinh(\Omega_2^*)}\right] \tag{26}$$

3 Results and Discussion

This study addresses the problem of the influence of the transport of stably stratified fluid driven by buoyancy force distribution through a vertical channel filled with anisotropic porous material. The problem is governed by a set of coupled partial differential equations decoupled using the D'Alembert method. Analytical solutions of the expressions for the momentum and the energy equations as well as the velocity gradients and volumetric mass flow rate were obtained and presented in the Laplace domain, which were then inverted to their corresponding time domain using a numerical algorithm based on Riemann sum approximation [15]. The variant responses of fluids with low and high Prandtl numbers such as air and water, respectively, to controlling physical quantities present in Eqs. (22)-(26) were analyzed and discussed.

3.1 Hydro and Thermo Dynamics Analysis

Subgraphs (a)-(d) of Figure 2 illustrate the thermal distribution in the channel with respect to the variation of time (t) and for various cases of buoyancy force distribution parameter (m^*). In all four cases examined, the thermal or temperature distribution is higher when the Prandtl number is low because fluids with low Prandtl numbers are better conductors of heat. In addition, subgraphs (a) and (b) of Figure 2 show that for $m^* = 0.0$ and $m^* = 1.0$, the impact of time on the thermal distribution in the channel is insignificant when time (t) is large for fluids with a low Prandtl number. Physically, this is a result of the steady state being attained as $t \to \Pr$. On the other hand, subgraphs (c) and (d) of Figure 2 show that at relatively small values of dimensionless time (t) and for fluids with high Prandtl numbers such as water, thermal distribution appears to attain relative stability near the center of the channel (between $y = 0.4$ and $y = 0.7$). This trend, though less pronounced in subgraph (c) of Figure 2, is indicated with line segments parallel to the transverse distance axis (y) when $t = 0.1$.

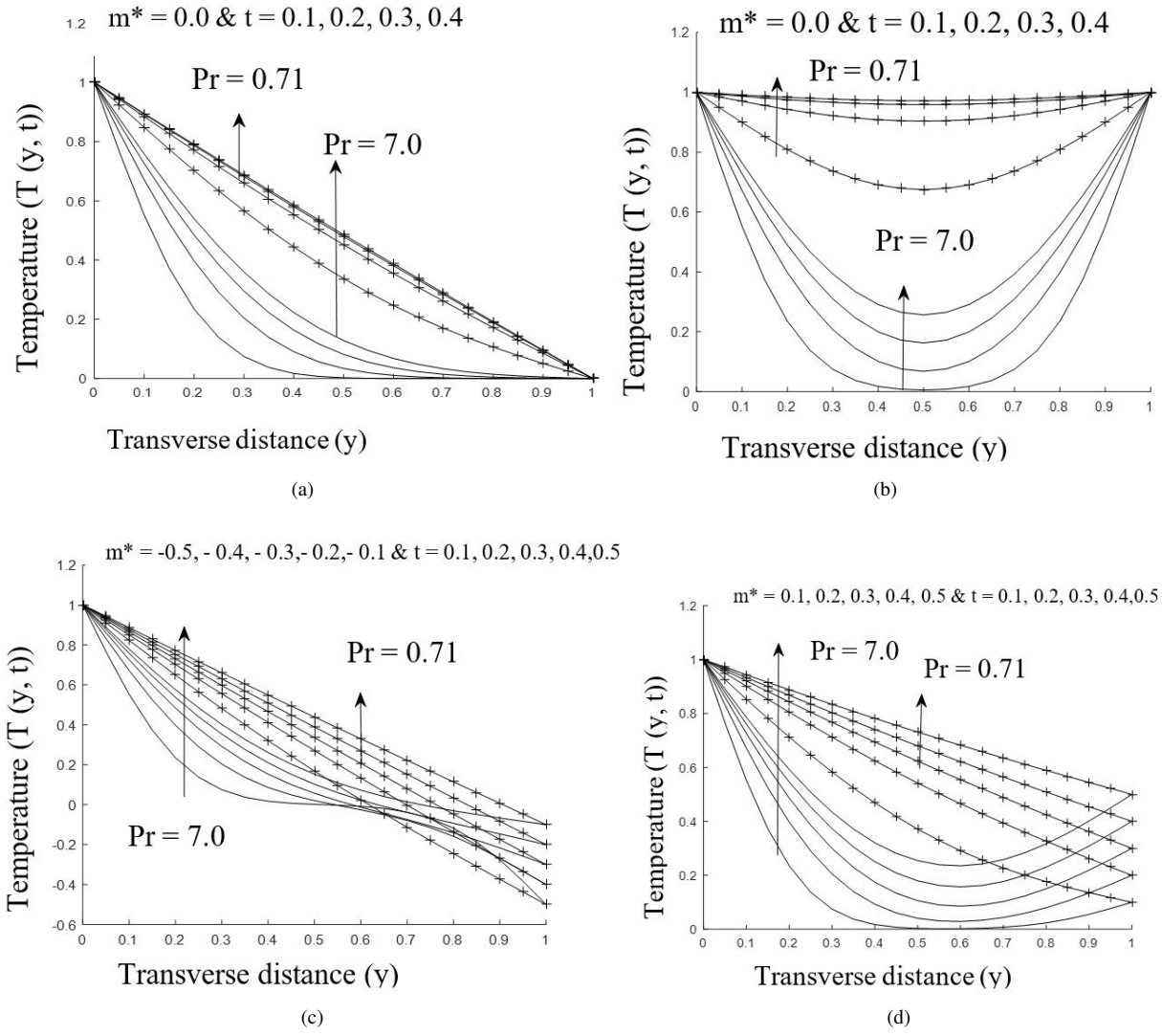

Figure 2. Temperature field with variation of buoyancy distribution term (m^*) and time (t) with $S = 2.0, Gr = 10.0, Da = 0.01, \gamma = 2.0, k^* = 0.4$ and $\theta = 60°$

Subgraphs (a)-(d) of Figure 3 depict the hydrodynamic distribution within the channel with respect to the variation of time (t) and for various cases of buoyancy force distribution parameter (m^*). For fluids with low Prandtl numbers like air, the figures show the occurrences of maximum fluid velocity close to the heated plate when $m^* = 0.0$ (subgraph (a) of Figure 3) and when $m^* < 0$ (subgraph (c) of Figure 3). The point of maximum velocity begins to drift toward the centerline of the channel when $0.1 < m^* < 0.5$ (subgraph (d) of Figure 3) and becomes fully centralized when $m^* = 1.0$ (subgraph (b) of Figure 3).

On the contrary, two different maxima velocities close to the plates are noticed for fluids with a high Prandtl

number, as seen in subgraphs (a), (b) and (d) of Figure 3, as the flow formation is found to be undulating in these figures. In addition, for both air $(\mathrm{Pr} = 0.71)$ and water $(\mathrm{Pr} = 7.0)$, the cooling of the fluid near the extreme plate $(y = 1)$ is observed to result in hydrodynamic reverse flow, as seen in subgraph (c) of Figure 3 when $m^* < 0$.

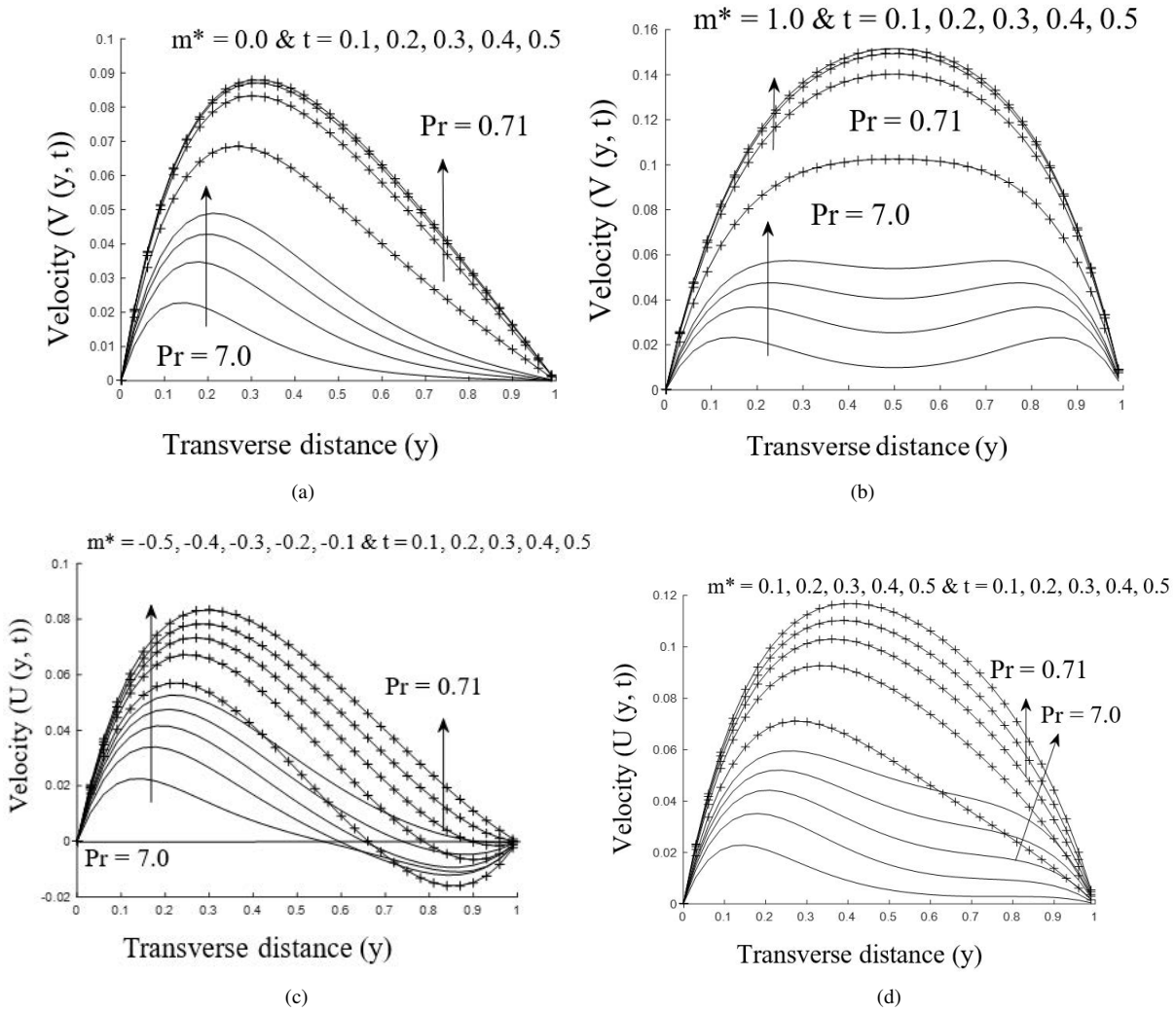

Figure 3. Velocity field with variation of buoyancy distribution term (m^*) and time (t) with $S = 2.0$, $Gr = 10.0, Da = 0.01, \gamma = 2.0, k^* = 0.4$ and $\theta = 60°$

Subgraphs (a)-(d) of Figure 4 and subgraphs (a)-(d) of Figure 5, respectively, present the impact of thermal stratification on fluid temperature and velocity for different cases of buoyancy force distribution parameter. In the classical case $(m^* = 0.0)$ and when $m^* = 1.0$, the impact of the layering effect in stalling temperature penetration and suppressing the strength of velocity current resulting from the variation in the thermal stratification is noticed in subgraphs (a) and (b) of Figure 4 with respect to temperature and subgraphs (a) and (b) of Figure 5 with respect to velocity for both air and water. While for $m^* < 0$ and $0.1 \leq m^* \leq 0.5$, subgraphs (c) and (d) of Figure 4, subgraphs (c) and (d) of Figure 5 reveal that the variation of the thermal stratification is observed to be initially insignificant, especially for air.

As the temperature and velocity distribution progress towards the cold plate, it can be seen that the layering effects of suppressing the temperature and the velocity distribution resulting from the increase in stratification are reversed. Furthermore, it can be observed that thermal and velocity reverse flows resulting from the cooling of the fluid near the cold plate commence quicker in the case of water $(\mathrm{Pr} = 7.0)$, as seen in subgraph (c) of Figure 4 and subgraph (c) of Figure 5, respectively.

Subgraphs (a)-(d) of Figure 6 and subgraphs (a)-(d) of Figure 7, respectively, compare the effect of the anisotropic angle of inclination on temperature penetration and the velocity current of the stratified fluid in the vertical channel. Evidently, the impact of the variation of the anisotropic angle of inclination with respect to different cases of buoyancy force distribution parameter is very significant because an increase in the anisotropic angle of inclination (θ) increases

the pore size of the anisotropic porous structures. This, in effect, decreases the conductivity strength of the porous matrix, and as such, a reduction in temperature penetration is noticed, as seen in subgraphs (a) and (b) of Figure 6, for both water and air. Interestingly, for $m^* < 0$ and $0.1 < m^* < 0.5$, as depicted respectively in subgraphs (c) and (d) of Figure 6, the effect of the variation of the anisotropic angle of inclination (θ) on the temperature penetration is initially insignificant for water. In addition, both figures show an increase in the conductivity strength of the porous structure for all the fluids considered and, therefore, enhance temperature distribution. On the other hand, the increase in the voids of the anisotropic porous medium by increasing its angle of inclination allows for more flow freedom for the fluid particles. This, interestingly, is the case, irrespective of the fluids taken into account and for all cases of the buoyancy distribution force parameters considered (subgraphs (a)-(d) of Figure 7). Additionally, the maximum velocity of the fluid was found near the hot plate (subgraphs (a) and (c) of Figure 7) and was then shifted to the center of the channel for air $(\mathrm{Pr} = 0.71)$, as observed in subgraph (b) of Figure 7, when $m^* = 1.0$. In addition, subgraphs (b) and (d) of Figure 7 show that the fluid $(\mathrm{Pr} = 7.0)$ attained two maximum velocities close to the plates when $m^* = 1.0$ and $0.1 \leq m^* \leq 0.5$. In addition, if $T_h < T_m < T_c$, the relative cooling of the fluid temperature close to the cold plate is ensured. Accordingly, reverse flow is observed for both fluids.

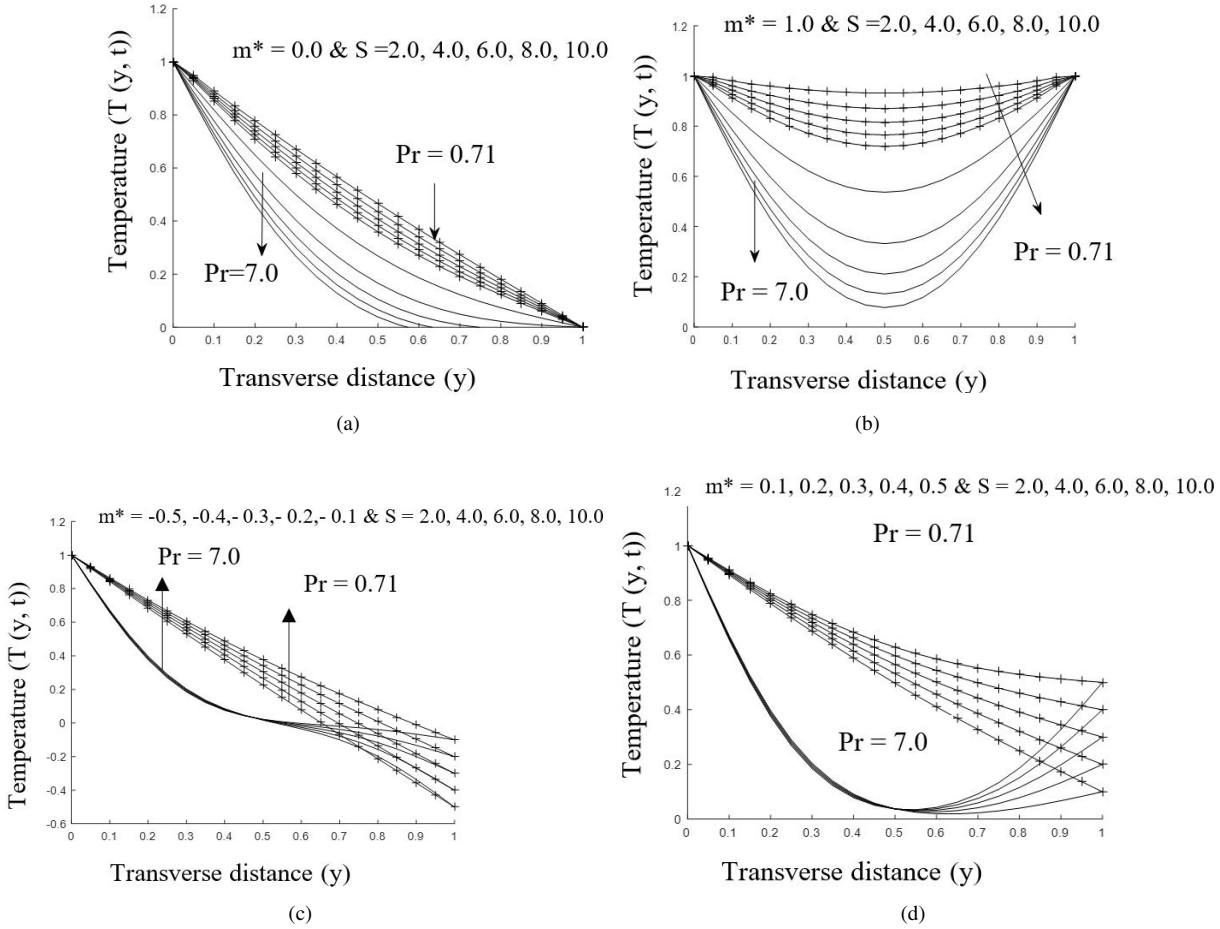

Figure 4. Temperature field with variation of buoyancy distribution term (m^*) and stratification parameter (S) with $t = 0.2, Gr = 10.0, Da = 0.01, \gamma = 2.0, k^* = 0.4$ and $\theta = 60°$

Subgraphs (a)-(d) of Figure 8 and subgraphs (a)-(d) of Figure 9, respectively, depict the response of the fluid temperature and velocity to the variation of the anisotropic ratio of permeability $\left(k^* = \frac{k_1}{k_2}\right)$ for various cases of buoyancy force distribution parameter (m^*). As k^* is increased, indicating the increase in the permeability along the vertical principal axis k_1 of the anisotropic porous matrix, the conductivity of the anisotropic porous structures is seen to be enhanced for all the fluids taken into account, as exhibited in subgraphs (a)-(d) of Figure 8. This trend is found, for water $(\mathrm{Pr} = 7.0)$, to be noticeably insignificant, as seen in subgraphs (c) and (d) of Figure 8, before the fluid temperature reaches the center of the channel $(y = 0.5)$.

On the fluid velocity, there is more flow along the horizontal permeability (k_2), as observed in the experimental investigation by Liakopoulos [19], which implies that increasing k^* suppresses the flow velocity along k_1 when

$m^* = 0, m^* = 1.0$ and $0.1 < m^* < 0.5$ and, therefore, a reduction in fluid velocity is observed. Furthermore, this reduction in the fluid velocity is also noticed in subgraph (c) of Figure 9. Reverse fluid flow is observed at the transverse distance between the plates $y = 0.6$ as a result of the relative cooling of the fluid temperature with respect to the temperature of the cold plate.

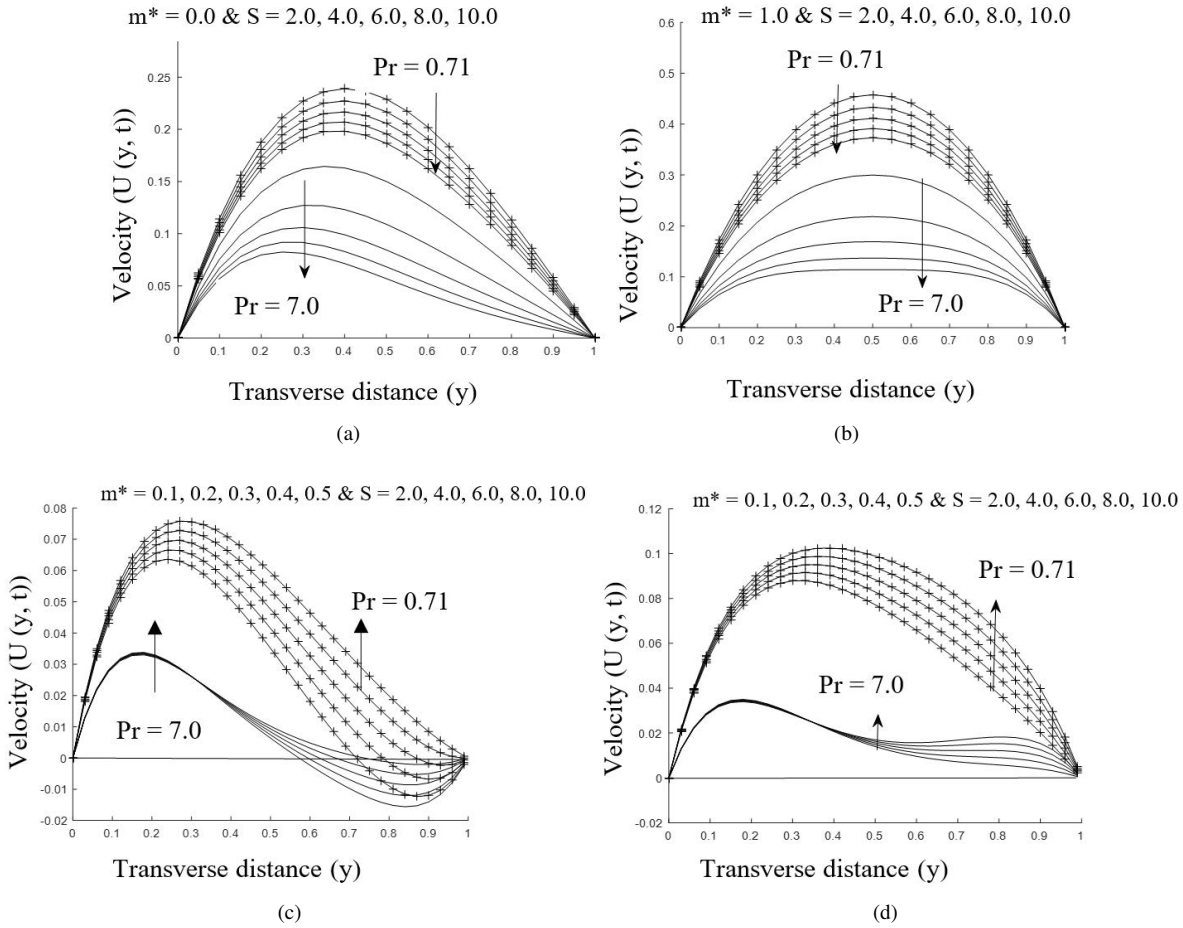

Figure 5. Velocity field with variation of buoyancy distribution term (m^*) and stratification parameter (S) with $t = 0.2, Gr = 10.0, Da = 0.01, \gamma = 2.0, k^* = 0.4$ and $\theta = 60^\circ$

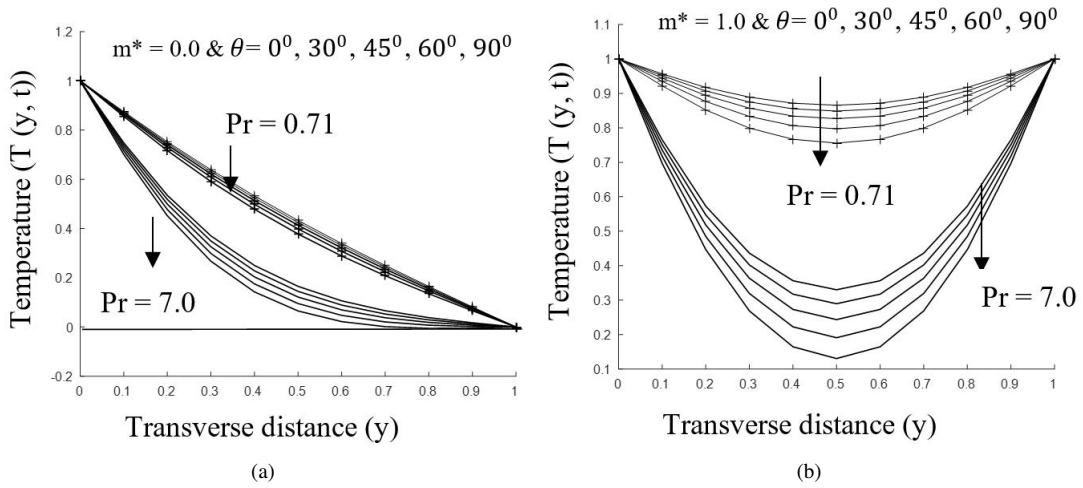

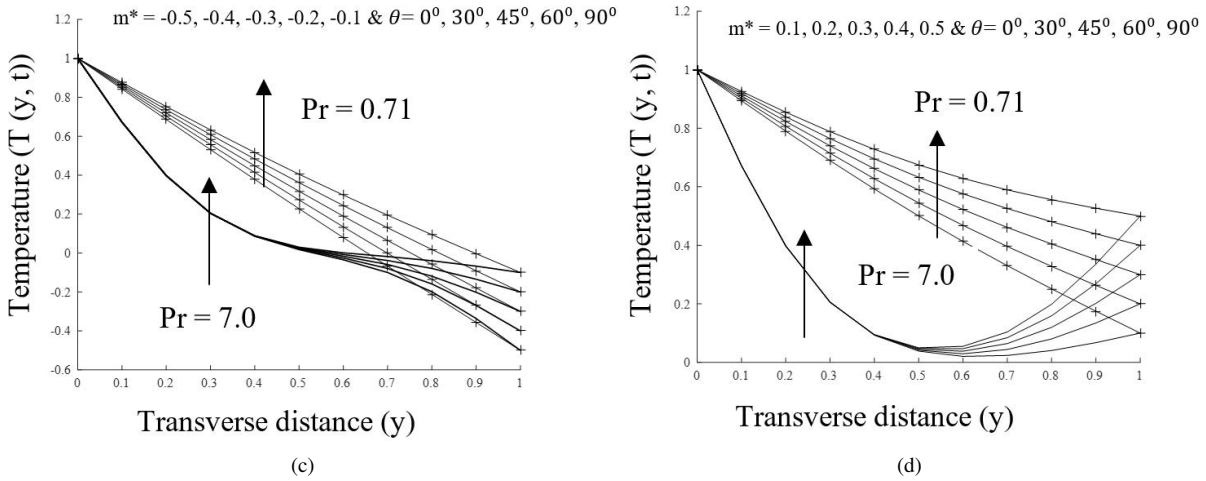

Figure 6. Temperature field with variation of buoyancy distribution term (m^*) and anisotropic angle of inclination (θ) with $t = 0.2, Gr = 10.0, Da = 0.01, \gamma = 2.0, k^* = 0.4$ and $\mathrm{S} = 2.0$

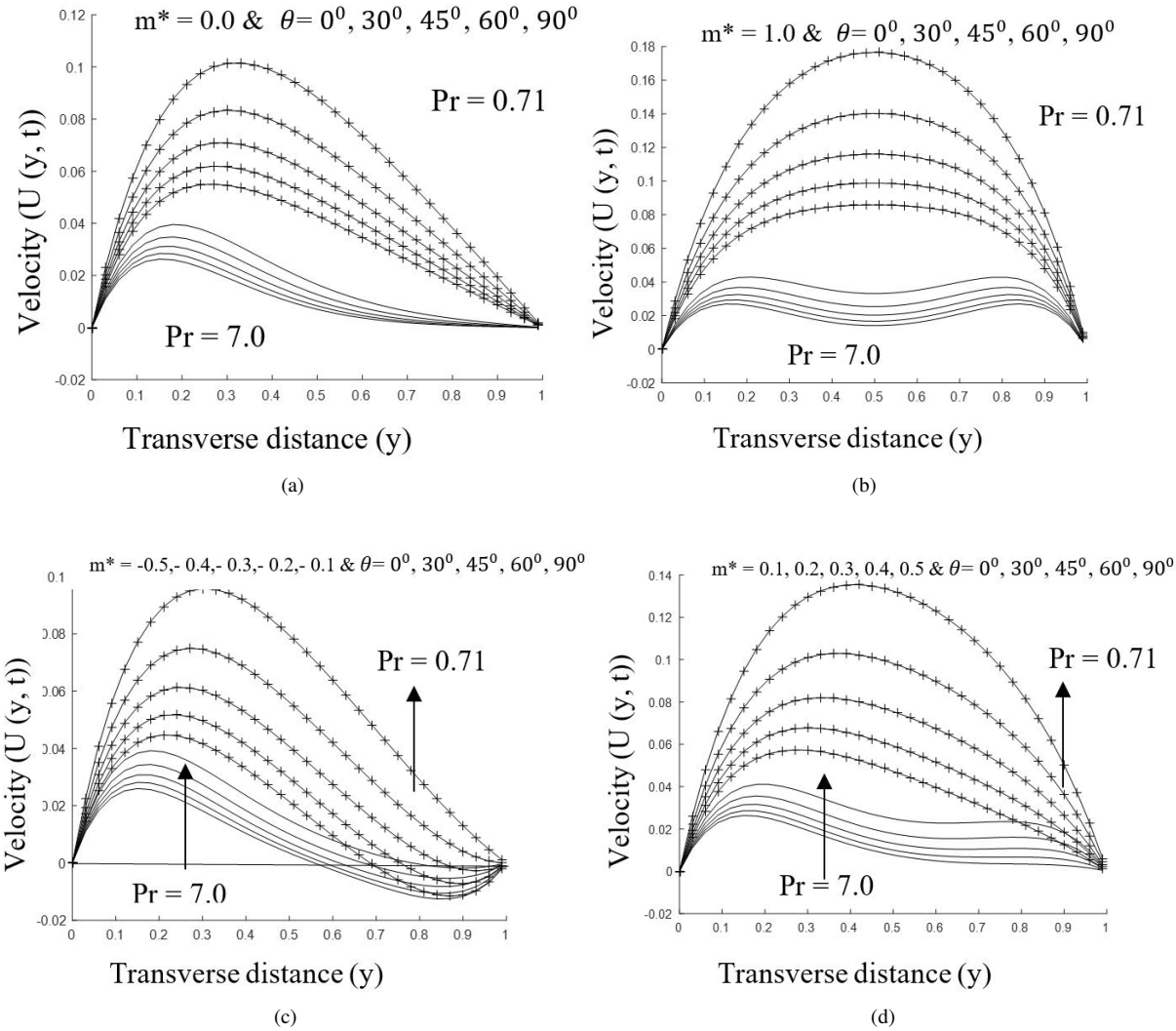

Figure 7. Velocity field with variation of buoyancy distribution term (m^*) and anisotropic angle of inclination (θ) with $t = 0.2, Gr = 10.0, Da = 0.01, \gamma = 2.0, \mathrm{k}^* = 0.4$ and $S = 2.0$

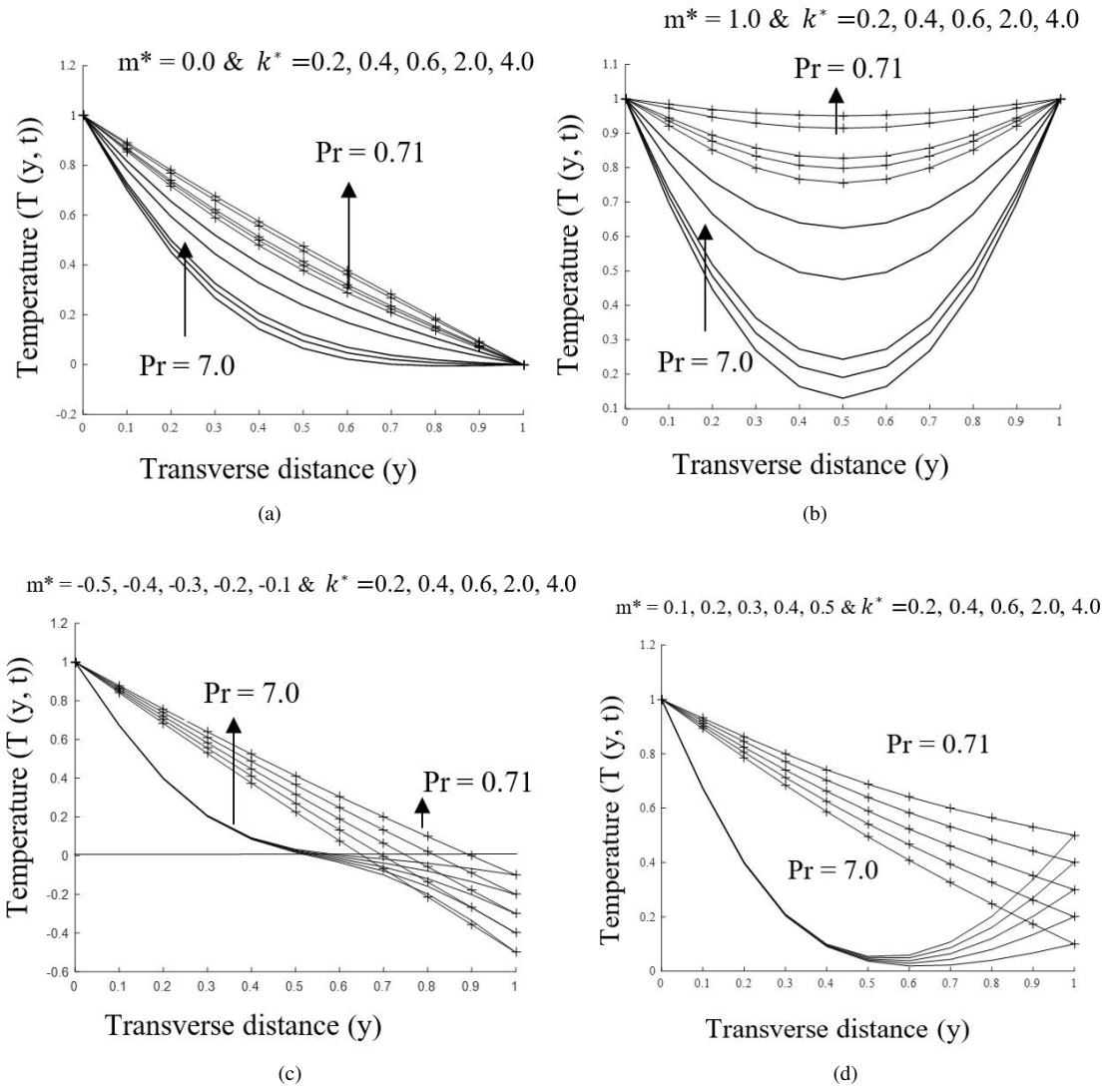

Figure 8. Temperature field with variation of buoyancy distribution term (m^*) and anisotropic permeability ratio (k^*) with $t = 0.2, Gr = 10.0, Da = 0.01, \gamma = 2.0, \theta = 60^\circ$ and $S = 2.0$

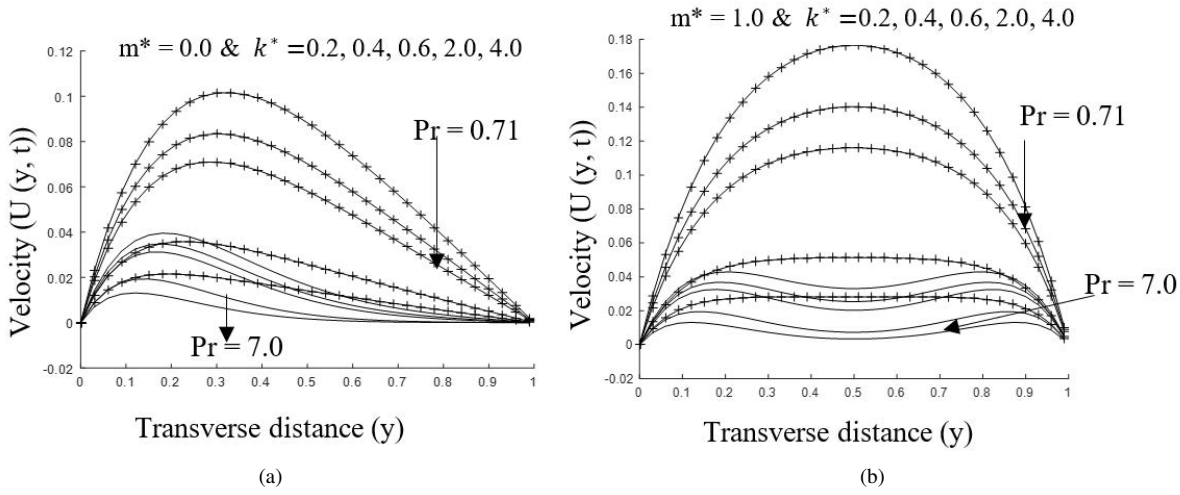

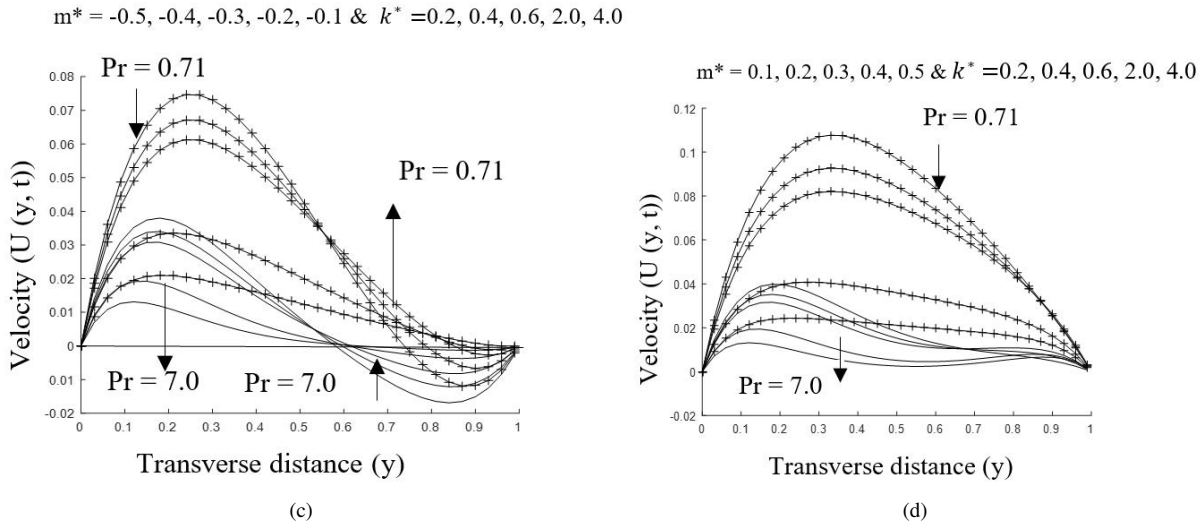

Figure 9. Velocity field with variation of buoyancy distribution term (m^*) and anisotropic permeability ratio (k^*) with $\mathrm{t} = 0.2, \mathrm{Gr} = 10.0, \mathrm{Da} = 0.01, \gamma = 2.0, \theta = 60^\circ$ and $\mathrm{S} = 2.0$

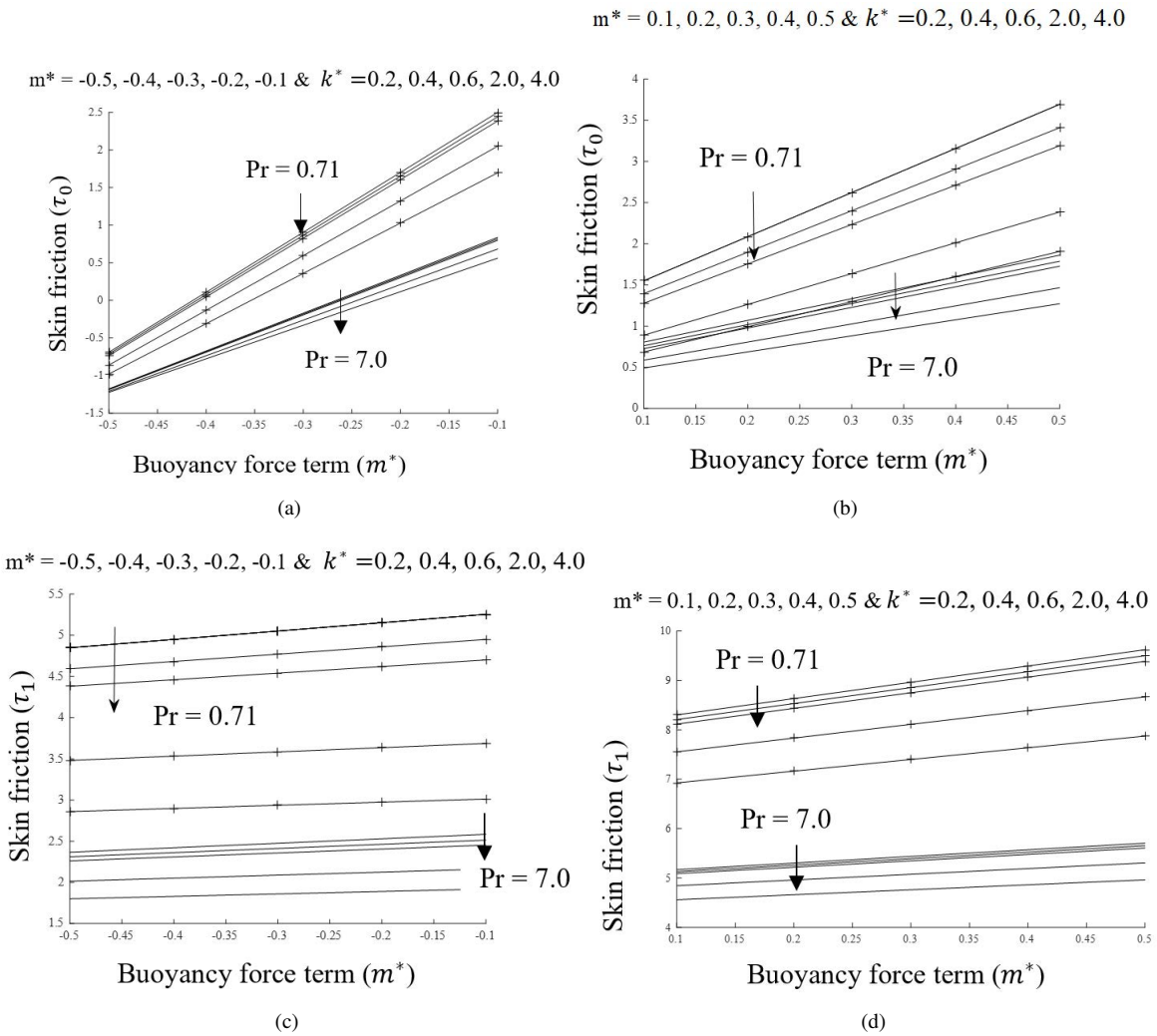

Figure 10. Skin friction with variation of buoyancy distribution term (m^*) and anisotropic permeability ratio (k^*) with $t = 0.2, Gr = 10.0, \mathrm{Da} = 0.01, \gamma = 2.0, \theta = 60^\circ$ and $S = 2.0$

3.2 Velocity Gradient and Mass Flow Rate Analysis

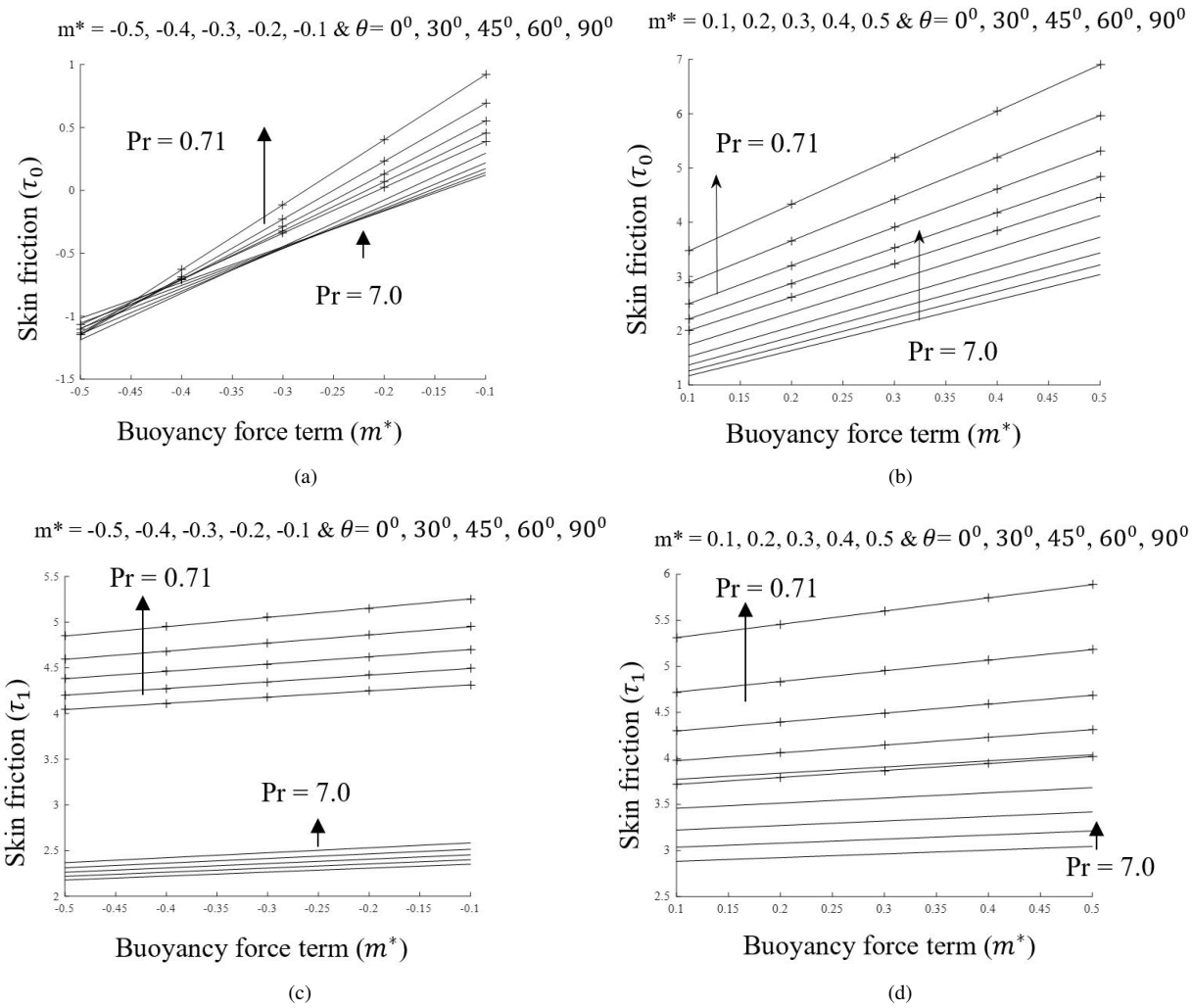

Figure 11. Skin friction with variation of buoyancy distribution term (m^*) and anisotropic angle of inclination (θ) with $t = 0.2, Gr = 10.0, Da = 0.01, \gamma = 2.0, k^* = 0.4$ and $S = 2.0$

The expressions for the velocity gradient or skin frictions $(\tau_0$ and $\tau_1)$ and volumetric mass flow rate are given by Eqs. (24), (25), and (26), respectively. This subsection discusses the effects of the stratification and the anisotropic parameters with respect to the variation buoyancy distribution force parameter on the skin friction at the inner surface of the hot wall and at the outer surface of the cold wall as well as on the volumetric mass flow rate. Subgraphs (a)-(d) of Figure 10, subgraphs (a)-(d) of Figure 11 and subgraphs (a)-(d) of Figure 12, respectively, display the skin friction with the variation of anisotropic permeability ratio (k^*), anisotropic angle of inclination (θ) and stratification parameter (S) for different cases of m^*. Generally, the figures indicate that there is mostly a buildup of friction at the surface of the cold wall. Furthermore, for all the cases of m^* being considered, the increase in the buoyancy distribution force aids the skin friction at both plates for both air and water. In particular, however, it is observed from subgraphs (a)-(d) of Figure 10 and subgraphs (a)-(d) of Figure 12 that increasing k^* and S, respectively, reduces the skin friction at the bounding plates. Physically, this behaviour can be attributed to the respective increase in the permeability of the anisotropic porous material vertically and the layering effect resulting from the increase in the stratification factor. On the contrary, it is noticed from subgraphs (a)-(d) of Figure 11 that increasing the anisotropic angle of inclination (θ) enhances the skin friction at both walls and for the two working fluids investigated.

In subgraphs (a) and (b) of Figure 13 and subgraphs (a) and (b) of Figure 14, irrespective of the working fluid, the volumetric mass flow is seen to be inhibited by increasing stratification factor (S) and anisotropic permeability ratio (k^*), respectively. This is because, due to the variation of the stratification parameter, the inherent layering effect of the stably stratified fluid hinders fluid motion and the rate of fluid flow per unit area. On the other hand, increasing the anisotropic permeability ratio (k^*) is akin to increasing the permeability of the porous medium vertically. This, as

already demonstrated, significantly reduces the fluid velocity and, subsequently, the volumetric mass flow as well. The numerical simulation conducted shows that the mass flow rate can be enhanced with an increase in the anisotropic angle of inclination (θ) for both air and water, as shown in subgraphs (a) and (b) of Figure 15.

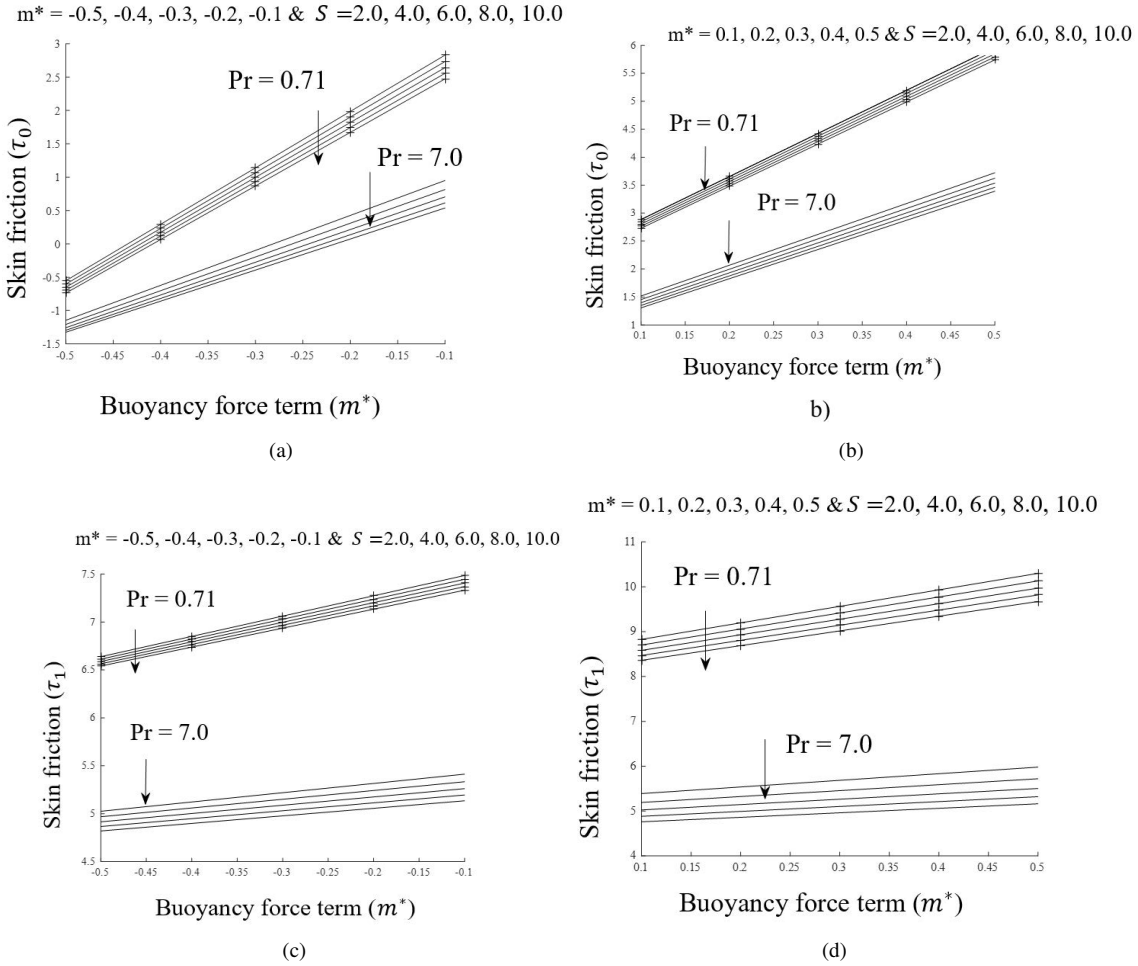

Figure 12. Skin friction with variation of buoyancy distribution term (m^*) and stratification parameter (S) with $t = 0.2, Gr = 10.0, Da = 0.01, \gamma = 2.0, k^* = 0.4$ and $\theta = 60°$

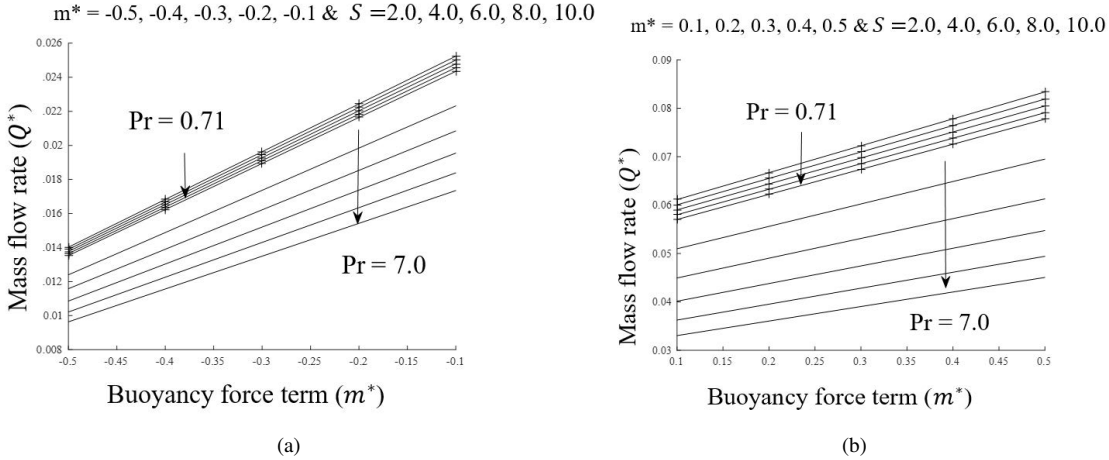

Figure 13. Mass flow rate with variation of buoyancy distribution term (m^*) and stratification parameter (S) with $t = 0.2, Gr = 10.0, Da = 0.01, \gamma = 2.0, k^* = 0.4$ and $\theta = 60°$

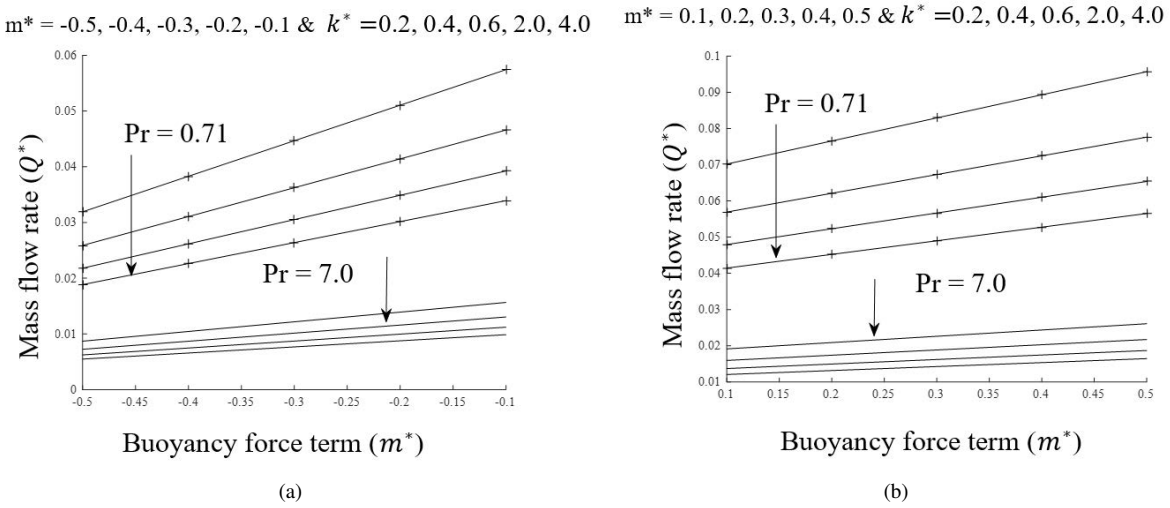

Figure 14. Mass flow rate with variation of buoyancy distribution term (m^*) and anisotropic permeability ratio (k^*) with $t = 0.2, Gr = 10.0, Da = 0.01, \gamma = 2.0, \theta = 60^\circ$ and $S = 2.0$

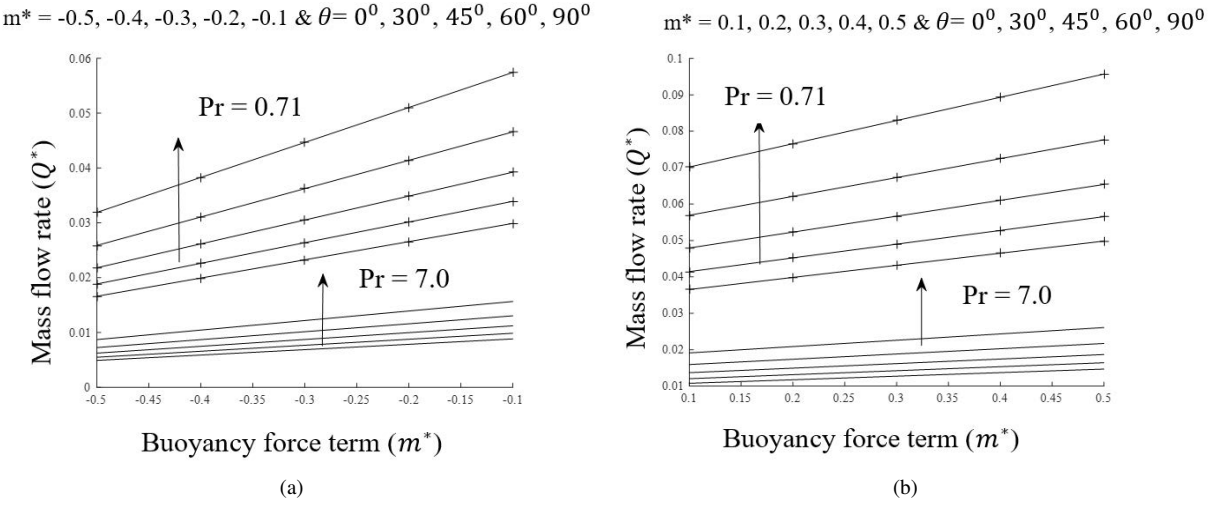

Figure 15. Mass flow rate with variation of buoyancy distribution term (m^*) and anisotropic angle of inclination (θ) with $t = 0.2, Gr = 10.0, Da = 0.01, \gamma = 2.0, \mathrm{k}^* = 0.4$ and $S = 2.0$

4 Conclusion

This study presents the result of the investigation of transient state natural convection of stratified fluid in an asymmetrically heated and cold vertical channel filled with anisotropic porous material. It primarily compares the effects of thermal stratification, anisotropic parameters and buoyancy force distribution parameters on fluids with high and low Prandtl numbers such as water (Pr = 7.0) and air (Pr = 0.71), respectively. The solutions of the fluid temperature and velocity profiles were obtained using three techniques: the Laplace transform technique, the D'Alembert (decoupling) method, and a numerical procedure based on Riemann sum approximation algorithms. This study in general shows the practicability of the combined effect of stratified fluid flow through an anisotropic porous medium, where the directional permeability can interact with the stratified layers to influence flow distribution and transport properties. However, the asymmetric heating/cooling of a porous material could lead to uneven expansion or contraction of the material, affecting the fluid flow patterns of the stratified fluid through the porous structure. Other inferences from the numerical simulation conducted include:

(i) If the fluid temperature is in between the different plates' temperatures, thermal and velocity reverse flows resulting from the cooling of the fluid near the cold plate can be observed and commence quicker in water $(Pr = 7.0)$.

(ii) An increase in k^* and S reduces the skin friction at the bounding plates for all cases of m^*. These trends result from the increase in the permeability of the anisotropic porous material vertically and the layering effect resulting

from the increase in the stratification factor, respectively.

(iii) On the other hand, it is noticed that an increase in the anisotropic angle of inclination (θ) enhances the skin friction at both walls and for the two working fluids investigated.

(iv) Finally, it is also established that the mass flow rate can be enhanced with an increase in the anisotropic angle of inclination (θ) and suppressed by increasing the anisotropic permeability ratio (k^*) and stratification parameter (S).

Future Research

This study examined the natural convection of stably stratified fluid by taking into consideration the anisotropic property of the porous structure via which the fluid flows and the orientation of the fluid temperature with the variant temperatures of the transport surfaces. Future work can be carried out by considering different models.

Researchers have constructed and worked on another form of porous media, the Bidisperse porous media [21]. The model suggested for the porous media is for isotropy and the fluid is non-stratified. It will be interesting if anisotropy, stratification and buoyancy force distribution terms are included in the extended Brinkman model for Bidisperse porous media. Since the resulting model is a set of coupled equations linking the fluid dynamics in the frictional and porous phases of the porous media, the methods used in the present study will be very helpful.

Data Availability

The data used to support the findings of this study are available from the corresponding author upon request.

Conflicts of Interest

The authors declare no conflict of interest.

References

[1] B. K. Jha, M. K. Musa, and A. O. Ajibade, "Effects of thermal stratification and anisotropic porous material in a symmetrically heated vertical channel," *SQUJS*, vol. 25, no. 2, pp. 112–123, 2020. https://doi.org/10.24200/squjs.vol25iss2pp112-123

[2] A. R. Khaled and K. Vafai, "The role of porous media in modeling flow and heat transfer in biological tissues," *Int. J. Heat Mass Transf.*, vol. 46, no. 26, pp. 4989–5003, 2003. https://doi.org/10.1016/S0017-9310(03)00301-6

[3] K. Govindaraju, S. Kamangar, I. A. Badruddin, G. N. Viswanathan, A. Badarudin, and N. S. Ahmed, "Effect of porous media of the stenosed artery wall to the coronary physiological diagnostic parameter: A computational fluid dynamic analysis," *Atherosclerosis*, vol. 233, no. 2, pp. 630–635, 2014. https://doi.org/10.1016/j.atherosclerosis.2014.01.043

[4] M. K. Das, P. P. Mukherjee, and K. Muralidhar, "Porous media applications: Biological systems," in *Modeling Transport Phenomena in Porous Media with Applications*, 2018, pp. 123–154. https://doi.org/10.1007/978-3-319-69866-3_5

[5] K. Khanafer and K. Vafai, "Applications of porous media in biological transport modeling," in *Modeling of Mass Transport Processes in Biological Media*, 2022, pp. 1–15. https://doi.org/10.1016/B978-0-323-85740-6.00014-5

[6] P. Bera and A. Khalili, "Double-diffusive natural convection in an anisotropic porous cavity with opposing buoyancy forces: Multi-solutions and oscillations," *Int. J. Heat Mass Transf.*, vol. 45, no. 15, pp. 3205–3222, 2002. https://doi.org/10.1016/S0017-9310(02)00024-8

[7] F. Li, J. Li, G. Xu, G. Liu, H. Kou, and L. Zhou, "Fabrication, pore structure and compressive behavior of anisotropic porous titanium for human trabecular bone implant applications," *J. Mech. Behav. Biomed. Mater.*, vol. 46, pp. 104–114, 2015. https://doi.org/10.1016/j.jmbbm.2015.02.023

[8] J. Garcia-Avila, E. Cuan-Urquizo, E. Ramírez-Cedillo, C. A. Rodríguez, and A. Vargad-Martinez, "Novel porous structures with non-cubic symmetry, elastic anisotropy, and fatigue life behavior," *Math. Mech. Solids*, vol. 28, no. 4, 2022. https://doi.org/10.1177/10812865221104236

[9] R. K. Deka and A. Paul, "Transient free convection flow past an infinite moving vertical cylinder in a stably stratified fluid," *J. Heat Transfer*, vol. 134, no. 4, p. 042503, 2012. https://doi.org/10.1115/1.4005205

[10] R. K. Deka and A. Paul, "Convectively driven flow past an infinite moving vertical cylinder with thermal and mass stratification," *Pramana J. Phys.*, vol. 81, no. 4, pp. 641–665, 2013. https://doi.org/10.1007/s12043-013-0604-6

[11] A. Shapiro and E. Fedorovich, "An analytical model of an urban heat island circulation in calm conditions," *Environ. Fluid Mech.*, vol. 19, pp. 111–135, 2019. https://doi.org/10.1007/s10652-018-9621-9

[12] M. Thebault, S. Giroux-Julien, V. Timchenko, C. Menezo, and J. Reizes, "Transitional natural convection in a vertical channel: Impact of the external thermal stratification," *Int. J. Heat Mass Transf.*, vol. 151, p. 119476, 2020. https://doi.org/10.1016/j.ijheatmasstransfer.2020.119476

[13] T. Ding, Z. M. Meng, K. Chen, G. M. Fan, and C. Q. Yan, "Experimental study on thermal stratification in water tank and heat characteristics of condenser in water-cooled passive residual heat system of molten salt reactor," *Energy*, vol. 205, p. 118052, 2020. https://doi.org/10.1016/j.energy.2020.118052

[14] H. Otto and C. Cierpka, "Influence of thermal stratification on vertical natural convection- experimental investigations on the example of thermal energy storage systems," *Phys. Fluids*, vol. 33, p. 083614, 2021. https://doi.org/10.1063/5.0056232

[15] B. K. Jha, M. K. Musa, and A. O. Ajibade, "Time dependent natural convection fluid flow of stably stratified fluid in an asymmetrically heated vertical channel filled with anisotropic porous material," *Heat Transf.*, vol. 52, no. 1, pp. 665–686, 2022. https://doi.org/10.1002/htj.22711

[16] A. K. Singh and T. Paul, "Transient natural convection between two vertical walls heated and cooled asymmetrically," *Int. J. Appl. Mech. Eng.*, vol. 11, no. 1, pp. 143–154, 2006.

[17] Y. Peng, H. K. Lee, D. S. Wu, and Y. Cui, "Bifunctional asymmetric fabric with tailored thermal conduction and radiation for personal cooling and warming," *Engineering*, vol. 10, pp. 167–173, 2022. https://doi.org/10.1016/j.eng.2021.04.016

[18] G. Degan, C. Akowanou, L. Fagbemi, and J. Zinsalo, "Hydrodynamic anisotropy effects on radiation-mixed convection interaction in a vertical porous channel," *Appl. Math.*, vol. 7, no. 1, pp. 22–39, 2016. https://doi.org/10.4236/am.2016.71003

[19] A. C. Liakopoulos, "Darcy's coefficient of permeability as symmetric tensor of second rank," *Hydrol. Sci. J.*, vol. 10, no. 3, pp. 41–48, 1965. https://doi.org/10.1080/02626666509493405

[20] Z. Recebli and H. Kurt, "Two-phase steady flow along a horizontal glass pipe in the presence of the magnetic and electrical fields," *Int. J. Heat Fluid Flow*, vol. 29, no. 1, pp. 263–268, 2007. https://doi.org/10.1016/j.ijheatfluidflow.2007.09.003

[21] B. K. Jha and M. K. Musa, "Steady state pressure driven fluid flow in a cylindrical tube filled with bidisperse porous medium," *Int. J. Heat Technol.*, vol. 36, no. 4, pp. 1423–1429, 2018. https://doi.org/10.18280/ijht.360434

Nomenclature

Da	Darcy number
k^*	Anisotropic ratio of Permeability
m^*	Buoyancy force distribution parameter
k_1 and k_2	Permeability along the principal axes of the anisotropic porous medium $\left(m^2\right)$
S'	Dimensional stratification parameter $\left(mK^{-1}\right)$
S	Dimensionless stratification parameter
Pr	Prandtl number
$\bar{T}$	Dimensionless temperature of the fluid in Laplace domain
T	Dimensionless temperature of the fluid in time domain
T'	Dimensional reference temperature (K)
T_0	Temperature of the plate at $y = 0\,(K)$
T_1	Temperature of the plate at $y = 1\,(K)$
t'	Dimensional time (s)
t	Dimensionless time
U'	Dimensional velocity of the fluid $\left(ms^{-1}\right)$
$\bar{U}$	Dimensionless fluid velocity in Laplace domain
U	Dimensionless fluid velocity in time domain
Q	Volumetric mass flow rate
Gr	Grashoff number
g	Acceleration due to gravity $\left(ms^{-2}\right)$
k	Thermal conductivity of the fluid
C_p	Specific heat of the fluid at constant pressure

Greek symbols

β	Coefficient of thermal expansion (K)
v_{eff}	Effective viscosity of the saturated anisotropic porous medium $\left(kgm^{-1}\ s^{-1}\right)$
v	Kinematic viscosity of the fluid
γ	Ratio of viscosities
θ	Anisotropic angle of inclination (Deg or Rad)
τ_0	Skin friction at $y = 0$
τ_1	Skin friction at $y = 1$